Large Eddy Simulation of Subsurface Phytoplankton Dynamics: An Optimum Condition for Chlorophyll Patchiness Induced by Langmuir Circulations

Ashley Brereton[a,*], Joseph Siddons[b], David Lewis[b]

[a] *National Oceanography Centre, Joseph Proudman Building, 6 Brownlow Street, Liverpool, L3 5DA, UK*
[b] *Department of Mathematics, University of Liverpool, United Kingdom, L69 7ZL*

Abstract

Phytoplankton patchiness occurs on a plethora of spatial and temporal scales which can be extremely patchy in both horizontal and vertical directions. This patchiness directly affects the dynamics of the overall bloom, so understanding the mechanisms for patchiness to occur on each scale is therefore integral to the understanding of plankton bloom dynamics as a whole. This modelling study aims to introduce a mechanism for patch formations, which has previously had very little exposure, but is ubiquitous to the oceanic mixed layer - patchiness induced by the interaction between nutrient upwelling and Langmuir circulations.

By combining a Large-Eddy Simulation which resolves Langmuir circulations, with an Nutrient-Phytoplankton-Zooplankton biological model, one can examine the horizontal and vertical patchiness which results from a flux of nutrients into the bottom of the mixed layer. Here, it is shown that phytoplankton form significant horizontal patchiness in a depth interval where vertical currents from Langmuir cells are apparent and turbulent mixing is not; this comprises the lower region of the surface mixed layer. Aggregations have frequently been observed in lower regions of the surface mixed layer and have been attributed to the high nutrient flux associated with the pycnocline. This modelling study also shows patches occurring in this region and it is hypothesised that Langmuir cells are a catalyst for patchiness. The results clearly demonstrate that for certain levels of

wind forcing, which are strong enough to introduce turbulent mixing only to the upper part of the mixed layer whilst inducing deeper Langmuir circulation, patchiness is greatly enhanced.
Keywords: Plankton Patchiness, Large-Eddy Simulation, Turbulence

1. Introduction

Wide ranging observations of plankton aggregations have been compiled over the last few decades (Gran & Braarud, 1935; Hulburt, 1968; Gohin et al., 2003; Dore et al., 2008). These formations have been detected on a wide range of spatial and temporal scales (Gallager et al., 2004; Mitchell et al., 2008; Siegel et al., 2002; Beman et al., 2005; Ryan et al., 2006; Martin, 2003). Phytoplankton aggregations are known to enhance growth rates (Mackas et al., 1985), so understanding the mechanisms behind patch formations can improve modelling forecasts of chlorophyll concentrations. A common behavioural trait of phytoplankton is that they aggregate over a relatively small depth interval of the surface mixed layer, e.g. Macías et al. (2013). This usually occurs below the mixing layer, a wind-driven surface layer of the water column which experiences with high turbulent mixing, but above the pycnocline, a deeper layer of the water column which experiences a large change in density over a small depth interval. This layer is generally laminar in nature. Many possible contributing factors have been postulated to explain these depth dependent patch formations. Examples include optimum nutrient/light levels, gyrotaxis and diel vertical migration (Durham & Stocker, 2012) and it is this depth dependent behaviour which is the main focus of this paper.

One of the main drawbacks of observational data is that full three-dimensional mappings are infeasible to obtain (mean depth profiles or surface satellite data are mainly produced). This means the biological profile is incomplete, a gap which can be filled by

*Corresponding author
Email address: ashbre@noc.ac.uk (Ashley Brereton)

the use of carefully prescribed mathematical models. Many modelling techniques have been employed to study the dynamics of phytoplankton blooms. Large scale bloom formation and planktonic patchiness has been investigated using large scale fluid models (Allen et al., 1999; Oschlies, 2002; Koné et al., 2009; Martin et al., 2002). However, the drawback of using these models is that the small scale phenomena is parameterised via a turbulent diffusion hypothesis and a hydrostatic assumption is commonly made. Though this is essential for permitting feasible spatial and temporal resolution for an ocean domain, it is limited by the current knowledge of the non-linear small scale processes. On the other side of the spectrum, the gold standard of computational fluid dynamics, known as Direct Numerical Simulation (DNS) has been used to explore the intricate dynamics of phytoplankton in turbulent flows (Durham et al., 2013; Zhan et al., 2014). Though this method is preferable, the domain size is limited (metres) due to the resolution scales needed, so is not practical for large scale applications. This naturally opens the field to a branch of modelling which captures the full 3D non-hydrostatic physics not captured in a primitive equation type models, whilst also permitting feasible resolution scales for ocean physics. This branch of modelling is known as Large-Eddy Simulation (LES).

Langmuir circulations have had little in the way of attention with regards to biological patchiness, although surface aggregates due to Langmuir circulations were first observed as far back as Charles Darwin's Beagle cruise of 1839 (Leibovich, 1983). Langmuir circulations control the mixing layer depth. In addition, the upwelling motions established by the onset of Langmuir turbulence pull nutrient rich waters up from the bottom of the mixed layer (Craik & Leibovich, 1976; McWilliams et al., 1997; Polton & Belcher, 2007; Thorpe, 2000). This promotes biological growth and has the potential to generate significant planktonic patchiness in regions of the water column where the local mixing is insufficient to disperse them. Hence, Langmuir circulations can act as an important physical stimulus to enhance biological activity. However, the detailed mechanism of this stimulus has not been studied in any detail and consequently it is poorly understood.

This paper will seek to address the interaction between Langmuir circulation and planktonic patchiness by using LES, as this is the only type of model suitable for resolving this particular phenomenon.

The biological model used in this work is a generic type Nutrient-Phytoplankton-Zooplankton (NPZ) model (Baird & Emsley, 1999; Lewis, 2005). Conceptually the NPZ model is slightly different from other three state NPZ models in the literature, e.g. Franks et al. (1986); Fasham et al. (1990); Edwards & Brindley (1996), in that a mechanistic approach has been adopted in the derivation in some of the terms (see model description). An important addition for this work is the inclusion of a non-uniform flux of nutrients into the bottom of the surface mixed layer. The LES is then coupled to the NPZ model to facilitate an investigation into the level of vertical and horizontal patchiness induced by the interaction between Langmuir circulations and the nutrient flux. This method of coupling an LES model to a biological model is a relatively new technique and a novel approach to the problem. Only a handful of authors have previously adopted this methodology to investigate the bio-physical dynamics (Lewis, 2005; Noh et al., 2006; Taylor & Ferrari, 2011). The work in this manuscript builds on the work of Lewis (2005) which, in contrast to this work, was not able to simulate biological time-scales (weeks) due to computational restrictions and did not include a non-uniform nutrient flux into the bottom of the mixed layer.

To summarise, this paper seeks to show that Langmuir circulations are an important driver for the formation of depth dependent biological patch formations. We will quantify both the horizontal and vertical phytoplankton patchiness which results from an interaction between a flux of nutrients into the bottom of the mixed layer and the presence of Langmuir circulations. The paper is set out as follows; Section 2 describes the model set-up and boundary conditions used to force the model. Section 3 comprises the main results of the model simulations, showing mixed layers subjected to different levels

of wind forcing and the resultant biological patchiness. Section 4 concludes the paper with a general discussion about the findings in section 3.

2. Model description

The mathematical framework used to study the bio-physical dynamics of the ocean boundary layer centres around the LES-NPZ model constructed by Lewis (2005). The workings of the model will be briefly outlined here.

The governing equations for the flow field used in this work comprise a version of the Navier-Stokes equations incorporating surface wave parameterisations, known as the Craik-Liebovich equations (Craik & Leibovich, 1976). They are expressed as follows;

$$\frac{D\boldsymbol{u}}{Dt} + f\hat{\boldsymbol{k}} \times (\boldsymbol{u} + \boldsymbol{U_S}) = -\frac{\nabla p}{\rho_0} + +\nabla \cdot \nu_T \nabla \boldsymbol{u} + \boldsymbol{U_S} \times \boldsymbol{\omega}, \tag{1}$$

Here $D/Dt \equiv \partial/\partial t + \boldsymbol{u} \cdot \nabla$, where $\boldsymbol{u}$ is the velocity field, f is the Coriolis frequency, $\boldsymbol{U_S}$ the Stokes drift velocity, $\boldsymbol{\omega} = \nabla \times \boldsymbol{u}$ the vorticity, $p = p_0 + \rho_0[2\boldsymbol{u} \cdot \boldsymbol{U}_S + |\boldsymbol{U}_S|^2]/2$ a generalized pressure term and ν_T is an eddy viscosity. Density and temperature are assumed to be constant in this model. The Stokes drift velocity is attributed to the presence of surface waves, which (without loss of generality) are directed along the x-axis. In which case $\boldsymbol{U}_S = (U_S e^{2kz}, 0, 0)$, where $U_S = \sigma k a^2$, a being the wave amplitude, k the wave number and $\sigma = \sqrt{gk}$ the wave frequency (Phillips, 1977). $\boldsymbol{u}$ and p are filtered in space and time, resulting directly from the spatial-temporal discretisation employed. Scales below the discretisation are modelled via the Smagorinsky scheme (Smagorinsky, 1963), which is an explicit eddy viscosity model.

Once the flow field has been calculated at a point in time, the results are then fed into the biological model, this is formulated as follows;

$$\frac{\partial N}{\partial t} + (\boldsymbol{u} + \boldsymbol{U_s}) \cdot \nabla N = D_T \nabla^2 N - N \text{ uptake by } P + N \text{ recycled from } P. \tag{2a}$$

$$\frac{\partial P}{\partial t} + (\boldsymbol{u} + \boldsymbol{U_s}) \cdot \nabla P = D_T \nabla^2 P + P \text{ growth from } N - P \text{ grazing loss.} \tag{2b}$$

$$\frac{\partial Z}{\partial t} + (\boldsymbol{u} + \boldsymbol{U_s}) \cdot \nabla Z = D_T \nabla^2 Z + Z \text{ growth from } P + Z \text{ mortality.} \tag{2c}$$

Here, D_T is the turbulent diffusivity of the respective scalar fields calculated by $D_T = \frac{\nu_T}{Sc}$, where Sc is a Schmidt number based on the resolution, for this setup Sc 0.5. The three non-dimensional scalar fields denoted by $N(\boldsymbol{x}, t) = N^*/N_0$, $P(\boldsymbol{x}, t) = P^*/P_0$ and $Z(\boldsymbol{x}, t) = Z^*/Z_0$ are representative of nutrient (specifically nitrate), phytoplankton and zooplankton (where N_0 in kg m^{-3}, P_0 and Z_0 in cells m^{-3} are suitable reference scales). The coupling between the LES flow field, calculated from Eq. 1 and the scalar quantities is represented by the second term in the equations. It is the assumption that the scalar fields are neutrally buoyant and are all treated as passive tracers, though it is acknowledged that buoyancy and swimming, for example, are tractable mechanisms for patch formations. The derivation of the functional forms of the source-sink terms can be quite involved, so for simplicity it was chosen to only state the functional forms in this work with only a brief description. First the uptake term is given by

$$N \text{ uptake by } P \ = 4\pi r_p Sh\,(\varepsilon, z)\, D_N N \left[1 - \frac{R_{N_0}(z)}{R_N^{\max}} N\right] P^*,$$

where r_p is a (spherical) radius of the phytoplankton cell, Sh is the turbulent Sherwood number, which is dependent on the energy dissipation rate ε. The latter is calculated directly from a preliminary LES simulation of the relevant boundary layer once statistical stationarity has been reached. The ratio $\frac{R_{N_0}(z)}{R_N^{\max}}$ represents the nitrate storage capacity of the cell to its maximum potential storage capacity. For the biological parameters employed here, this ratio ≈ 0.5 and hence whenever $N > 2$, nutrient uptake falls to zero. Since r_p is usually less than the associated Kolmogorov microscale, ε plays a diminished role in the uptake term. The next two terms consist of

$$N \text{ recycled from } P \ = (1-\beta_E)\,\frac{s_N P^*}{N_0}\mu_p^{\max} e^{\alpha z} \min\left[1, \frac{R_{N_0}(z)}{R_N^{\max}} N\right],$$

$$P \text{ growth from } N \ = \beta_E \mu_p^{\max} e^{\alpha z} \min\left[1, \frac{R_{N_0}(z)}{R_N^{\max}} N\right] P.$$

Here $\beta_E \in (0,1]$ represents the growth efficiency of the phytoplankton species, s_N is the stoichiometry co-efficient, α is the light attenuation co-efficient of water and $\mu_p^{\max}$ represents the maximum growth rate achievable by the phytoplankton species. The next two predation terms are given by

$$P \text{ grazing loss } \ = J\left(R, T_R, \epsilon, \sigma_Z\right) Z^* P,$$

$$Z \text{ growth from } P \ = \min\left[\mu_Z^{\max}, J\left(R, T_R, \epsilon, \sigma_Z\right) Y P^*\right] Z.$$

Here $J\left(R, T_R, \epsilon, \sigma_Z\right)$ represents the predation rate of a single predator possessing a spherical perception field of radius R. T_R is the reaction time of the zooplankton species and σ_Z is the swimming speed of the species. Y is the amount of new zooplankton cells created per phytoplankton cell captured and $\mu_Z^{\max}$ is the maximum growth rate, see (Lewis & Pedley, 2001) for detailed discussion of the functional form of J. ε has a much larger effect on the predation rate than it does on the phytoplankton uptake rate, since R $(1-40)$mm is substantially larger than the Kolmogorov microscale. Turbulence increases the number of predator prey contacts, usually leading to an enhancement of the predation rate. Finally, the equations are closed by the mortality term given by

$$Z \text{ mortality } \ = \mu_Z^{\text{death}} Z.$$

Here μ_Z^{death} is a constant death rate of the zooplankton species.

For an extensive analysis of the NPZ model, including stability analysis, ε dependent parameters, comparison to the full LES-NPZ model and for a full list of parameter values used, alongside analysis of the physical LES model directly relevant to the simulations

performed in this work see Lewis et al. (2017).

2.1. Boundary conditions for the LES-NPZ model

For this study, a series of turbulent boundary layers were generated, each characterised by the values of the Stokes drift velocity U_S, and the friction velocity U_*. The latter determines the wind stress boundary condition applied at the surface

$$\nu_T \frac{\partial u}{\partial z}\bigg|_{z=0} = \frac{\tau}{\rho_0} = U_*^2. \tag{3}$$

Here τ is the surface wind stress. Values of U_* were varied between $1.5 - 5.0 \times 10^{-3}\text{ms}^{-1}$, roughly equivalent to wind-speeds of $U_{10} = 1.2 - 4.0\text{ms}^{-1}$ at 10 metres above the sea surface. The corresponding values of U_S were based on a constant Langmuir number $La = \sqrt{\frac{U_*}{U_s}} = 0.3$, a value which corresponds to a fully developed sea (McWilliams et al., 1997; Harcourt & D'Asaro, 2008; Sullivan et al., 2012). Typically, the various boundary layers were spun up from rest for a period $\tau_{spin} \approx 17\text{hrs}$, until a quasi-equilibrium state was reached before any biological fields were added.

Velocity and pressure fields were computed from equations (1) over a computational domain 120m $\times$ 120m horizontally and to a depth of $z_{ml} = 33\text{m}$, where z_{ml} is the mixed (distinct from the mixing) layer depth, utilising a basic grid of $40 \times 40 \times 75$. This implies a regular resolution scale of $\Delta x = \Delta y = 3\text{m}$ and $\Delta z = 0.45\text{m}$ (although the vertical resolution was stretched to give greater resolution near the sea surface to resolve the log layer sufficiently). Horizontal periodicity is enforced at the lateral boundaries. At the surface, $w = 0$ and zero stress imposed on v. No-slip condition are imposed at $z = z_{ml}$. Lateral periodic boundary conditions are imposed for all scalar quantities. Furthermore, zero flux boundary conditions are imposed for all scalar quantities at the surface and for P and Z at the bottom boundary.

For the nutrient field, Williams & Follows (1998) suggest a positive uniform nutrient flux should be of the order 2×10^{-8}mol N m^{-2}s^{-1} which is roughly equivalent to $\langle wN^* \rangle = 2.8 \times 10^{-10}$kgm^{-2}s^{-1}, which helps replenish nutrient losses due to phytoplankton growth. However, this paper is concerned with the possible formation of PZ patchiness in the mixed layer, starting from initially uniform distributions, which can only occur in response to some form of stimulus. The most likely stimulus that could initiate such a response would be a localised surge of nutrients into the mixed layer. This would influence the growth rates of a wide cross section of phytoplankton species, which, after some lag time, would in turn produce a response higher up the planktonic food chain. Such a nutrient surge might be the result of a heavy river run off or via a sustained up-welling gyre forcing nutrient rich deep water into the mixed layer, for example. Vertical fluxes of nutrients also occur naturally when momentum shear associated with internal tides facilitates turbulent mixing and the conversion of barotropic tidal energy to baroclinic dissipation at the pycnocline (Sandstrom & Elliott, 1984; Sharples et al., 2007). Rines et al. (2010) report observations in Monterey Bay, CA in which patchy horizontal phytoplankton distributions were correlated with the frequency of large-scale, nutrient rich, advection events. Furthermore, patchy distributions of phytoplankton have been observed and correlated to high frequency internal waves (Lennert-Cody & Franks, 1999). However, for this study the exact mechanism of the nutrient surge is not particularly important. One is much more interested in its potential effects. To mimic an upwelling event, a localised non-uniform flux of nutrients through the base of mixed layer was introduced throughout the duration of a simulation. A pocket of turbulence generated via internal wave mixing will advect nutrient rich water upwards. It will then have to travel through a laminar band of water between the pycnocline and the mixing layer, making the dynamics of the nutrient upwelling diffusive. Therefore a diffusive flux is imposed near the bottom of the mixed layer. Mathematically this boundary condition

takes the form

$$\frac{D_T}{2.8\times10^{-10}}\frac{\partial N}{\partial z}\bigg|_{z=-z_{ml+}} = 1 + Qexp\left[\frac{-(x^2+y^2)}{2\sigma_{xy}^2}\right]. \tag{4}$$

Here (x, y) represents the horizontal co-ordinates with $-60\text{m} \leq x \leq 60\text{m}$ and $-60\text{m} \leq y \leq 60\text{m}$, Q is the strength of the nutrient flux at the centre and $\sigma_{xy} > 0$ a length scale that governs the spatial extent of the nutrient surge. Note that as a no-slip boundary condition is imposed at the base of the mixed layer, the nutrient surge is imposed one grid-point above the base of the mixed layer, denoted by z_{ml+}. For most of these simulations values of $Q = 130$ and $\sigma_{xy} = 7.6\text{m}$ were chosen. This creates a highly localised source, some hundred times the background. The source is localised because a value of $\sigma_{xy} = 7.6\text{m}$ ensures that outside a circle of radius 25m or so from the centre, the nutrient flux value falls back to within a few percent of its background level. Here spatial extent of the nutrient source is on the length scale associated with that of a high-frequency internal wave (Boegman et al., 2003). However, as will be demonstrated later, the spatial extent of this nutrient flux does not have a qualitative effect on the solutions. Even if a uniform nutrient flux is prescribed, only relatively minor changes to the levels of patchiness in the phytoplankton distribution are brought about (see the subsequent discussion surrounding Fig. 9). Since the uptake term switches off whenever $N > 2$, there is a cap as to how much extra P growth such a source with stimulate. With the strength of the source imposed, $N > 2$ is reached within 2 days at all points in the domain, which means that the phytoplankton perceive the nutrient field as homogeneous after this time. The nutrient field itself has no cap imposed, but any nutrient concentration with a value of $N > 2$ has no additional effect to phytoplankton growth. Initial conditions of $P_0 = Z_0 = 0.5$ and $N_0 = 1$ were chosen so that biological oscillations would be initiated in and around the co-existence equilibrium point $\left(\hat{N}, \hat{P}, \hat{Z}\right) = (1.56, 0.43, 0.85)$, see Lewis et al. (2017) for details. An important point concerning the limit cycles of the predator-prey dynamics is that while they may not mimic reality, they do produce periodic phytoplankton blooms. The work carried out is concerned with the spatial heterogeneity brought on during a

phytoplankton bloom and while the time scale and periodicity of the bloom may not be realistic, the spatial patchiness produced should depend much more on the flow field dynamics. A time-frame that is feasible for the LES to simulate is roughly 3-4 weeks due to the computationally expensive nature of LES. A limit cycle timescale was chosen to be 10 days to capture at least two phytoplankton blooms, the initial bloom being highly likely to depend (spatially) on the homogeneous initial conditions prescribed.

3. Results

To try and establish how planktonic patchiness is influenced by the physical forcings driving the boundary layer, one needs to assess both the lateral patchiness and the depth dependent patchiness. One can do this by introducing the (lateral) patchiness intensity measure;

$$I(U_*, z, t) = \frac{< P'^2 >}{< P >^2}. \tag{5}$$

Here $<>$ denotes a horizontal average, such that $< P > + P' = P$. This measure is similar to other metrics used in many previous works to measure biological patchiness (Reigada et al., 2003; Fessler et al., 1994; Lewis, 2005; Durham et al., 2011). Notice that when $< P >$ is close to zero, I is very large by definition, but this is of little interest. To mitigate this, a filter is applied to I when $< P >$ falls below a threshold of 0.1 - a value deemed small. The filtered measure is defined as

$$I(U_*, z, t) = 0 \qquad\qquad < P > \; < \; 0.1.$$

One can average I over a simulation time i.e.

$$I_{av}(U_*, z) = \frac{1}{T} \int_0^T I dt \tag{6}$$

to locate the depth at which $I_{av}(U_*, z)$ is maximised i.e. $\max_z[I_{av}(U_*, z)] = I_{av}(U_*, z_{opt})$. A series of simulations were run for different U_* and $I_{av}(U_*, z_{opt})$ was computed across each boundary layer. The results are shown in Fig. 1.

One can see from Fig. 1 that there is a peak in patchiness intensity at an intermediate wind stress of $U_* = 3.5 \times 10^{-3}\text{ms}^{-1}$ and then the signal decreases as the wind stress increases. From these results, it is clear that values of $U_* \geq 4 \times 10^{-3}\text{ms}^{-1}$ do not permit significant patch formations as the turbulent mixing spans the mixed layer completely. $U_* = 4 \times 10^{-3}\text{ms}^{-1} = U_{crit}$ will be deemed critical for the generation of significant patchiness. There is also only a small signal for low wind stress values, which suggests that

there is insufficient levels of mixing to promote patchiness. As $U_* \to 0$ the flow field will tend towards stagnation. In this regime, the only form of transport will be molecular diffusivity (eddy-diffusivity will be zero due to zero shear in the flow field). In this regime, nutrient concentrations will disperse and spread out in all directions, meaning relatively high concentrations of nutrients will not be sustained in laterally localised regions of the water column. Hence from the definition I_{av} will tend to zero over time. This finding is initially counter-intuitive, as one might expect patchiness to decrease monotonically as the wind speed (and hence turbulent mixing) is increased. However, for lower wind speeds, vertical currents are not as prevalent and hence nutrients near the bottom of the mixed layer cannot be advected up the water column effectively to facilitate strong patchiness. To understand the behaviour of $I_{av}\left(z_{opt}\right)$ a little better, it is necessary to investigate how $< P(z,t) >$ varies with depth.

Fig. 2 shows that for low (Fig. 2a) and intermediate (Fig. 2b) levels of wind forcing, biological oscillations are out of phase and exhibit different amplitudes. This demonstrates that the phytoplankton communities are not well mixed across the mixed layer and behave according to their local (biological) depth dependant parameters. This is likely to be an indicator for the formation of biological patchiness, as it reveals that high levels of turbulent mixing are not present to homogenise the scalar fields over the mixed layer. For high levels of wind forcing (Fig. 2c) however, the biological dynamics become independent of depth. Concentration fields at all depths merge into a single oscillation, indicating that micro-organisms are being vigorously mixed throughout the boundary layer. This type of behaviour will be termed 'phase locking'. Although it can't be seen in Figs. 2a and 2b, a certain proportion of curves near to the surface fall on top of each other, indicating there is a subset depth interval near the surface which is also phase locked. One sees a wider spread of concentrations for the low wind stress, compared to the medium wind stress case. This can be explained for the low wind case, by there being a larger non 'phase-locked' depth range at which the biological model is prominent

over the physical model. This larger spread of concentrations leads one to believe that horizontal heterogeneity must also be larger, but this is not necessarily the case. One can consider a zero wind case where the flow is static. In this case, every depth would be out of phase owing to parameters such as depth dependant light levels etc. In this case, the concentrations would experience a maximum spread of different population dynamics, but there would be no lateral dependant terms to induce horizontal patchiness. This means that for horizontal patchiness to form, there must be a certain amount of mixing to generate nutrient transport laterally at a particular depth, but at the same time the mixing cannot be so strong as to drive the system into phase-locked mode. To demonstrate this vertical homogenisation (phase-locking), one can use another measure analogous to that of the patchiness intensity in Eq. 6. This is defined by

$$I_z(U_*) = \frac{1}{MK} \sum_{j=1}^{K} \sum_{i=1}^{M} \frac{(< P(z_i, t_j) > - \check{P}(t_j))^2}{\check{P}(t_j)^2}, \tag{7}$$

where

$$\check{P}(t_j) = \frac{1}{M} \sum_{i=1}^{M} < P(z_i, t_j) > . \tag{8}$$

I_z is a metric describing the level of heterogeneity across the mixed layer, K is the reciprocal of the sampling frequency and M is the number of vertical grid points. So for example, if $I_z = 0$ then the biology is in a completely phase locked mode. Fig. 3 shows that for wind stress values of $U_* \geq U_{crit}$, the biology is effectively phase locked, as I_z is very small. This supports the hypothesis that phase locking correlates strongly with horizontal homogenisation.

Here, the statistics which have been used to diagnose biological patchiness only give a general idea of the amount of mixing throughout the entire boundary layer. They do not provide any insight into the depth dependence of the turbulent mixing. This can be examined by using the phytoplankton as a proxy, to show how the wind and wave

forcing influence the boundary layer mixing depth, i.e. how penetrative it is. Although phytoplankton are subject to both growth and decay, they are still passive with respect to the flow and can act in the role of a tracer. Fig. 4 shows that for low wind stress (Fig. 4a) $< P >$ concentrations do not change with depth within the top 10 metres or so of the boundary layer, demonstrating that the turbulence is strong enough to mix this portion of the boundary layer, but no more. Concentrations below this point are much more variable, indicating that the dynamics are primarily governed by the depth dependent biological parameters (light levels, nutrients etc). At an intermediate wind stress value $U_* = 3.5 \times 10^{-3}\text{ms}^{-1}$ (Fig. 4b), there is enough turbulence to mix down to approximately 25 metres of the boundary layer, as $< P >$ remains uniform up until this point. This example is important, as it indicates that mixing is taking place close to the bottom of the mixed layer where nutrient replenishment is imposed. Finally, for high wind stress values $U_* \geq U_{crit}$ (Fig. 4c) the biology is completely mixed, as there is no depth dependence in concentration and the biological dynamics are not strong enough to overcome the physical forcing mechanism. Note, that in all graphs shown in Fig. 4 the depth at which homogeneity ceases is independent of time.

One can use the behaviour of $< P >$ profiles to ascertain a mixing depth, z_{mix} for all simulated U_* values. Let

$$z_{mix} = min_z \left[var_t(P_z) > 10^{-3} \right], \tag{9}$$

where $P_z = \frac{\partial < P >}{\partial z}$ and var_t represents a variance taken across all time outputs. In this expression an arbitrary threshold value of 10^{-3} is given and the shallowest depth (given by the min_z operator) at which the logical expression is true is termed the mixing depth, z_{mix}. In other words, z_{mix} is the depth at which $< P >$ profiles cease to be uniform (and hence mixed) with depth. Fig. 8a shows a plot of z_{mix} against U_*. The monotonic deepening of the mixing layer is observed and one can surmise that a laminar band of water lies between this curve and z_{ml}. One expects to find appreciable patchiness between

z_{mix} and z_{ml} and homogenised plankton concentrations above z_{mix}. Note that once $z_{mix} = z_{ml}$ at $U_* \geq U_{crit}$, no patch formations are likely. This metric also correlates well with levels of vertical velocity variance, a measure of the strength of the vertical turbulence kinetic energy and hence the strength of the Langmuir cells (Fig. 8b), where surface boundary layer thickness clearly increases monotonically with wind stress until the behaviour levels off at $U_* \geq U_{crit}$ when the mixing depth reaches the mixed layer depth.

To illustrate further how the phytoplankton concentrations react to wind forcing, one can assess the levels of lateral heterogeneity to determine the depths at which patch formations are most likely to form. For this purpose, it is easiest to use the metric $I_{av}(U_*, z)$ defined in Eq. 6. Figs. 6a and 6c both show that lateral patchiness is unlikely to occur at either low or high levels of wind forcing. However, if the wind stress is set to an intermediate level, as shown in Fig. 6b, a much stronger signal emerges. One sees that patches accumulate around 25m, within the laminar band, where turbulent mixing ceases to dominate the system (see Fig. 4b).

Fig. 7 shows a snapshot, taken taken at z_{opt} at a point in time in which the patchiness intensity is high at an intermediate friction velocity of $U_* = 3.5 \times 10^{-3} ms^{-1}$. What is most striking is the structure of the horizontal patches, in that they are closely correlated to the structure of the Langmuir cells. Fig. 7d shows Langmuir cells manifesting themselves as a series of upwellings and downwellings (see McWilliams et al. (1997); Lewis (2005) for details) . Note the angular deflection of the Langmuir cells from the wind direction, this is due to inertial oscillations instigated by the rotation term in the momentum equations (Lewis & Belcher, 2004; Polton et al., 2005). Fig. 8 shows a vertical cross section, again at a point in time at which patchiness intensity is high. Upwelling zones and downwelling zones can be seen in the NPZ distributions and clearly demonstrates the mechanism of Langmuir cells advecting nutrient rich waters into upwelling

zones and inducing horizontal patchiness. This also indicates that the structure of the phytoplankton community is dependent on the flow field and not on the geometric extent of the imposed nutrient flux boundary condition. To verify this assertion, two control runs were completed, both using the same physical and biological parameters and the same average nutrient flux into the boundary layer, with varying distributions of the nutrient flux. It is unlikely for any patchiness to be observed in the high wind forcing case. In the low wind cases, the laminar band between the bottom boundary and the mixing layer will be large and so the nutrient dynamics will be more diffusive, effectively smoothing out the influence of the geometry of the bottom nutrient boundary condition. Therefore, the decisive scenario occurs when the wind forcing is intermediate. Hence tests were conducted with $U_* = 3.5 \times 10^{-3} ms^{-1}$. One simulation was prescribed with a Gaussian nutrient pump as described in section 2.1 and the other prescribed with a laterally uniform nutrient flux. Fig. 9 shows the resultant I_{av} for both cases. The crucial point is that, although the uniform flux results in a somewhat lower average patchiness intensity, the depth at which it is maximum is consistent. The quantitative differences seen are caused by nutrients being advected towards their closest upwelling region in the Gaussian pump case. This results in relatively rapid phytoplankton growth over a relatively small region, leading to high intensity signatures. By contrast, in the uniform case the nutrients have no preference for the particular upwelling region, so the resulting growth is less intense and less localised. Nevertheless it is still sufficient to produce a significant intensity signature within the laminar band. These results indicate that patch formations remain robust, irrespective of the geometric set up of the nutrient boundary condition. There is no correlation between the latter and the structure of the patch formations. Instead, patchiness occurs where nutrients are transported (not where it originates), and the nature of the transport is regulated by the Langmuir cell structure induced by the wind forcing. Furthermore, it shows that Langmuir circulations are taking control of the distribution of the biological fields, separating them into two distinct populations of upwelling and downwelling inhabitants.

This correlation of planktonic patchiness with Langmuir circulations is reinforced by the result of two similar boundary layer simulations. One boundary layer was driven purely by wind forcing and no surface wave effects (Fig. 10a) and one Langmuir circulation run driven by both wind and surface wave forcing terms (Fig. 10b). Each figure shows the correlation $< w'P' >$ of the vertical velocity and the phytoplankton field. Fig. 10b shows a strong correlation signal around the mixing depth z=25m in the Langmuir simulation, which is completely absent in the purely wind driven case. These experiments show clearly that Langmuir circulations are directly responsible for the strong depth dependent patchiness presented in this work. This is a surprising result as the presence of Langmuir circulations would imply a much more energetic boundary layer compared to the wind driven case, which would intuitively imply destruction of heterogeneity. But instead they can, under the right conditions, produce enhanced biological structure.

4. Discussion

Phytoplankton patchiness is a ubiquitous feature of near surface ocean boundary layers. The work carried out in this paper attempts to establish under what conditions patchiness is likely to occur in. In simple terms, this paper demonstrates that a compromising amount of surface forcing (through wind and waves) is required to induce patchiness signatures. If forcing is too weak, the flow field is quiescent and upwellings aren't set up to pull nutrients up into laterally heterogeneous zones. If forcing is too strong, the whole boundary layer becomes turbulent and concentrations become vigorously mixed and homogenised throughout.

The optimum condition for biological patchiness occurs when surface forcing is at an intermediate level, not too strong, nor too weak. When this level is achieved, the upper portion of the boundary layer becomes vigorously mixed and the lower portion becomes quasi-quiescent with established upwellings (and downwellings). This means that in the laminar band, between z_{mix} and z_{ml}, nutrients are advected upwards into laterally heterogeneous zones whilst the lateral mixing mixing is insufficient to disperse the resultant patchiness. Langmuir circulations are of key importance to this process, as they penetrate quite deeply into the mixed layer, creating zones of high vertical mixing combined with relatively low lateral transport. So any biological patches that accrue through growth tend to remain relatively heterogeneous. It was also found that the mechanism by which nutrients are injected into the mixed layer does not have a profound effect on the patchiness in terms of the depth at which patchiness is formed. However, if the spatial extent of the nutrient source is small enough, advection into closest upwelling zones is likely, skewing the patchiness distribution and increasing the patch signature. This is an important result, as nutrient surges come in a wide range of spatio-temporal scales. Finally, it should be noted that the frequency of the limit cycles in the plankton population dynamics is overly idealised, due to the simplicity of the biological model. To test the dependence of the limit cycle behaviour on horizontal patchiness, one should

make use of a more realistic biological model.

Future work will be carried out to ascertain if there is a natural scaling between the depth and strength of phytoplankton patchiness, the depth at which nutrients are injected into a system and the mixing depth associated with different levels of wind and wave forcing. Furthermore, with new insights into how populations of phytoplankton populations may separate out into upwelling and downwelling zones when Langmuir circulations are present, work will be undertaken to investigate plankton bloom duration when subjected to different levels of wind and wave forcing.

Acknowledgement

The authors would like to thank Dr Jeff Polton and Dr Rachel Bearon for their time spent proof reading the manuscript, their insights proved invaluable to the work and the authors are beyond grateful for that. The authors would also like to warmly thank the anonymous reviewers, whose comments made a large positive impact on the manuscript as a whole. This work was funded by the Natural Environment Research Council (grant reference number NE/D01073X/1).

Allen J, Howland R, Bloomer N, Uncles R (1999) Simulating the spring phytoplankton bloom in the humber plume, uk. Marine Pollution Bulletin 37:295–305

Baird ME, Emsley SM (1999) Towards a mechanistic model of plankton population dynamics. Journal of Plankton Research 21:85–126

Beman JM, Arrigo KR, Matson PA (2005) Agricultural runoff fuels large phytoplankton blooms in vulnerable areas of the ocean. Nature 434:211–214

Boegman L, Imberger J, Ivey GN, Antenucci JP (2003) High-frequency internal waves in large stratified lakes. Limnology and oceanography 48:895–919

Craik AD, Leibovich S (1976) A rational model for langmuir circulations. Journal of Fluid Mechanics 73:401–426

Dore JE, Letelier RM, Church MJ, Lukas R, Karl DM (2008) Summer phytoplankton blooms in the oligotrophic north pacific subtropical gyre: Historical perspective and recent observations. Progress in Oceanography 76:2–38

Durham WM, Climent E, Barry M, De Lillo F, Boffetta G, Cencini M, Stocker R (2013) Turbulence drives microscale patches of motile phytoplankton. Nature communications 4

Durham WM, Climent E, Stocker R (2011) Gyrotaxis in a steady vortical flow. Physical Review Letters 106:238102

Durham WM, Stocker R (2012) Thin phytoplankton layers: characteristics, mechanisms, and consequences. Annual review of marine science 4:177–207

Edwards AM, Brindley J (1996) Oscillatory behaviour in a three-component plankton population model. Dynamics and stability of Systems 11:347–370

Fasham M, Ducklow H, McKelvie S (1990) A nitrogen-based model of plankton dynamics in the oceanic mixed layer. Journal of Marine Research 48:591–639

Fessler JR, Kulick JD, Eaton JK (1994) Preferential concentration of heavy particles in a turbulent channel flow. Physics of Fluids 6:3742–3749

Franks P, Wroblewski J, Flierl G (1986) Behavior of a simple plankton model with food-level acclimation by herbivores. Marine Biology 91:121–129

Gallager SM, Yamazaki H, Davis CS (2004) Contribution of fine-scale vertical structure and swimming behavior to formation of plankton layers on georges bank. Marine ecology Progress series 267:27–43

Gohin F, Lampert L, Guillaud JF, Herbland A, Nézan E (2003) Satellite and in situ observations of a late winter phytoplankton bloom, in the northern bay of biscay. Continental shelf research 23:1117–1141

Gran HH, Braarud T (1935) A quantitative study of the phytoplankton in the bay of fundy and the gulf of maine (including observations on hydrography, chemistry and turbidity). Journal of the Biological Board of Canada 1:279–467

Harcourt R, D'Asaro E (2008) Large-eddy simulation of langmuir turbulence in pure wind seas. Journal of Physical Oceanography 38:1542–1562

Hulburt EM (1968) Phytoplankton observations in the western caribbean sea. Bulletin of Marine Science 18:388–399

Koné V, Aumont O, Lévy M, Resplandy L (2009) Physical and biogeochemical controls of the phytoplankton seasonal cycle in the indian ocean: A modeling study. Indian Ocean Biogeochemical Processes and Ecological Variability :147–166

Leibovich S (1983) The form and dynamics of langmuir circulations. Annual Review of Fluid Mechanics 15:391–427

Lennert-Cody CE, Franks PJ (1999) Plankton patchiness in high-frequency internal waves. Marine Ecology Progress Series :59–66

Lewis D (2005) A simple model of plankton population dynamics coupled with a les of the surface mixed layer. Journal of theoretical biology 234:565–591

Lewis D, Belcher S (2004) Time-dependent, coupled, ekman boundary layer solutions incorporating stokes drift. Dynamics of Atmospheres and Oceans 37:313–351

Lewis D, Brereton A, Siddons J (2017) A large eddy simulation study of the formation of deep chlorophyll/biological maxima in un-stratified mixed layers: The roles of turbulent mixing and predation pressure. Limnology and Oceanography

Lewis D, Pedley T (2001) The influence of turbulence on plankton predation strategies. Journal of Theoretical Biology 210:347–365

Macías D, Rodríguez-Santana Á, Ramírez-Romero E, Bruno M, Pelegrí JL, Sangrà P, Aguiar-González B, García CM (2013) Turbulence as a driver for vertical plankton distribution in the subsurface upper ocean. Scientia Marina 77:541–549

Mackas DL, Denman KL, Abbott MR (1985) Plankton patchiness: biology in the physical vernacular. Bulletin of Marine Science 37:652–674

Martin A (2003) Phytoplankton patchiness: the role of lateral stirring and mixing. Progress in oceanography 57:125–174

Martin AP, Richards KJ, Bracco A, Provenzale A (2002) Patchy productivity in the open ocean. Global Biogeochemical Cycles 16

McWilliams JC, Sullivan PP, Moeng CH (1997) Langmuir turbulence in the ocean. Journal of Fluid Mechanics 334:1–30

Mitchell JG, Yamazaki H, Seuront L, Wolk F, Li H (2008) Phytoplankton patch patterns: seascape anatomy in a turbulent ocean. Journal of Marine Systems 69:247–253

Noh Y, Kang I, Herold M, Raasch S (2006) Large eddy simulation of particle settling in the ocean mixed layer. Physics of Fluids 18:085109

Oschlies A (2002) Can eddies make ocean deserts bloom? Global Biogeochemical Cycles 16

Phillips O (1977) The dynamics of the upper ocean cambridge university press. New York

Polton JA, Belcher SE (2007) Langmuir turbulence and deeply penetrating jets in an unstratified mixed layer. Journal of Geophysical Research Oceans 1978 2012 112

Polton JA, Lewis DM, Belcher SE (2005) The role of wave-induced coriolis–stokes forcing on the wind-driven mixed layer. Journal of Physical Oceanography 35:444–457

Reigada R, Hillary RM, Bees MA, Sancho JM, SaguÃĺs F (2003) Plankton blooms induced by turbulent flows. Proceedings of the Royal Society of London Series B Biological Sciences 270:875–880

Rines J, McFarland M, Donaghay P, Sullivan J (2010) Thin layers and species-specific characterization of the phytoplankton community in monterey bay, california, usa. Continental Shelf Research 30:66–80

Ryan JP, Ueki I, Chao Y, Zhang H, Polito PS, Chavez FP (2006) Western pacific modulation of large phytoplankton blooms in the central and eastern equatorial pacific. Journal of Geophysical Research Biogeosciences 2005 2012 111

Sandstrom H, Elliott J (1984) Internal tide and solitons on the scotian shelf: A nutrient pump at work. Journal of Geophysical Research Oceans 89:6415–6426

Sharples J, Tweddle JF, Mattias Green J, Palmer MR, Kim YN, Hickman AE, Holligan PM, Moore C, Rippeth TP, Simpson JH, et al. (2007) Spring-neap modulation of internal tide mixing and vertical nitrate fluxes at a shelf edge in summer. Limnology and Oceanography 52:1735–1747

Siegel D, Doney S, Yoder J (2002) The north atlantic spring phytoplankton bloom and sverdrup's critical depth hypothesis. science 296:730–733

Smagorinsky J (1963) General circulation experiments with the primitive equations: I. the basic experiment*. Monthly weather review 91:99–164

Sullivan PP, Romero L, McWilliams JC, Melville WK (2012) Transient evolution of langmuir turbulence in ocean boundary layers driven by hurricane winds and waves. Journal of Physical Oceanography 42:1959 – 1980

Taylor JR, Ferrari R (2011) Shutdown of turbulent convection as a new criterion for the onset of spring phytoplankton blooms. Limnol Oceanogr 56:2293–2307

Thorpe S (2000) Langmuir circulation and the dispersion of oil spills in shallow seas. Spill science technology bulletin 6:213–223

Williams RG, Follows MJ (1998) The ekman transfer of nutrients and maintenance of new production over the north atlantic. Deep Sea Research Part I Oceanographic Research Papers 45:461–489

Zhan C, Sardina G, Lushi E, Brandt L (2014) Accumulation of motile elongated micro-organisms in turbulence. Journal of Fluid Mechanics 739:22–36

List of Figures

1 Optimum patchiness intensity $I_{av}\,(z_{opt})$, taken for a range of wind stress values. 24
2 Dynamics of phytoplankton and zooplankton concentrations calculated from the model. The solid (green) lines show phytoplankton concentration at each depth level and the dotted (red) lines show the zooplankton concentrations also across all depth levels. A comparison was made between a low wind stress ($U_* = 2 \times 10^{-3}\text{ms}^{-1}$), an intermediate wind stress ($U_* = 3.5 \times 10^{-3}\text{ms}^{-1}$), and a high wind stress ($U_* = 5 \times 10^{-3}\text{ms}^{-1}$). This figure serves to illustrate the phase locking effect (across depth) at high wind forcing. 25
3 Relationship between the level of wind stress subjected to the boundary layer and the level of (scaled) variance between phytoplankton concentrations at each depth, averaged over time. The lower the variance, the more 'phase locked' the system is in terms of depth dependent heterogeneity. . 26
4 Depth profiles of $< P >$ at instantaneous points in time. The dotted (blue) line shows the profile after 3 days, the solid (green) line shows the profile at 10 days and the dashed (red) line shows the profile at 17 days. A comparison was made between a low wind stress ($U_* = 2 \times 10^{-3}\text{ms}^{-1}$), a moderate wind stress ($U_* = 3.5 \times 10^{-3}\text{ms}^{-1}$), and a high wind stress ($U_* = 5 \times 10^{-3}\text{ms}^{-1}$). 27
5 Mixing depth varying as a function of wind speed. Note here that for $U_* \geq U_{crit}$ and the vertical velocity variance $< w^2 >$ against depth, indicating vertical turbulent kinetic energy where lighter shades indicate higher energetics. 28
6 I_{av} (the quantification of lateral patchiness strength) ranging from low to high wind stress regimes. This illustrates the optimum condition for phytoplankton patchiness. 29
7 Snapshot of Z, P, N and w at z_{opt} for an intermediate wind stress value of $U_* = 3.5 \times 10^{-3}\text{ms}^{-1}$ 30
8 Nutrient, Phytoplankton and Zooplankton concentrations after 12 days of simulation time, when the Phytoplankton community are starting the bloom phase of the limit cycle. Here $U_* = 3.5 \times 10^{-3} ms^{-1}$ 31
9 Graph of the time averaged patchiness intensity I_{av} against depth for $U_* = 3.5 \times 10^{-3} ms^{-1}$. The blue dotted line indicates a simulation prescribed by the Gaussian nutrient pump used in this work and the green solid line indicates a simulation prescribed by a uniform nutrient pump. 32
10 $< w'P' >$ for $U_* = 3.5 \times 10^{-3}\text{ms}^{-1}$. The left panel shows the correlation between vertical currents and Phytoplankton concentration with Langmuir circulations switched off and the right panel has Langmuir circulations switched on. 33

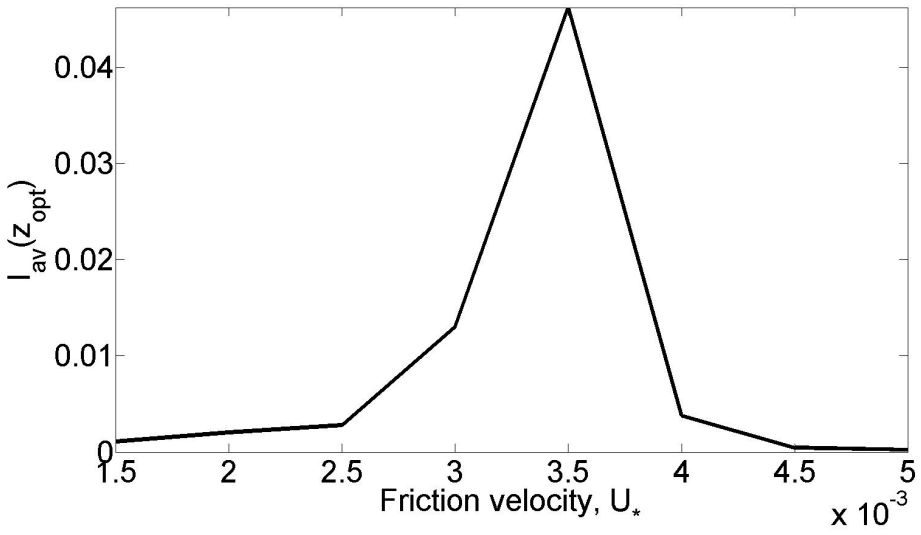

Figure 1: Optimum patchiness intensity $I_{av}\,(z_{opt})$, taken for a range of wind stress values.

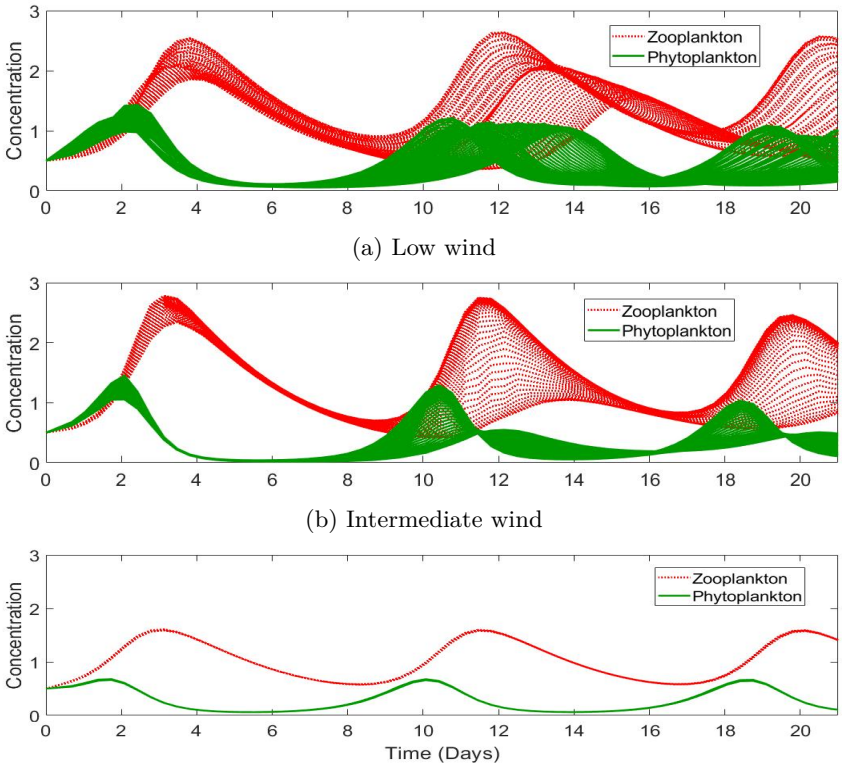

(a) Low wind

(b) Intermediate wind

(c) High wind

Figure 2: Dynamics of phytoplankton and zooplankton concentrations calculated from the model. The solid (green) lines show phytoplankton concentration at each depth level and the dotted (red) lines show the zooplankton concentrations also across all depth levels. A comparison was made between a low wind stress ($U_* = 2 \times 10^{-3} \mathrm{ms}^{-1}$), an intermediate wind stress ($U_* = 3.5 \times 10^{-3} \mathrm{ms}^{-1}$), and a high wind stress ($U_* = 5 \times 10^{-3} \mathrm{ms}^{-1}$). This figure serves to illustrate the phase locking effect (across depth) at high wind forcing.

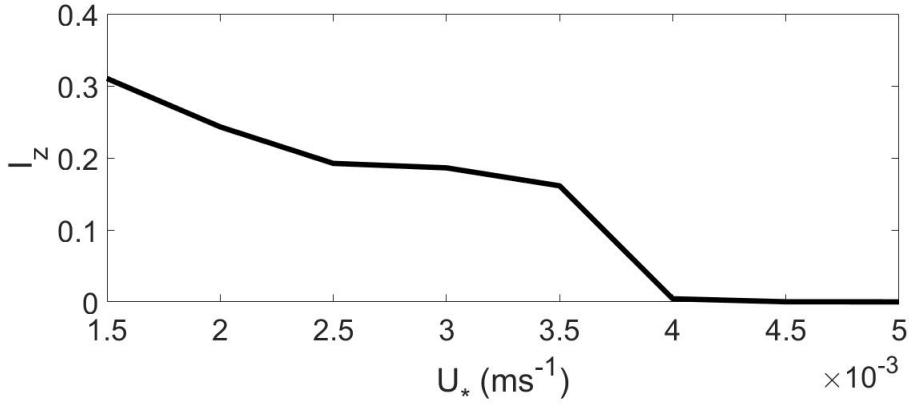

Figure 3: Relationship between the level of wind stress subjected to the boundary layer and the level of (scaled) variance between phytoplankton concentrations at each depth, averaged over time. The lower the variance, the more 'phase locked' the system is in terms of depth dependent heterogeneity.

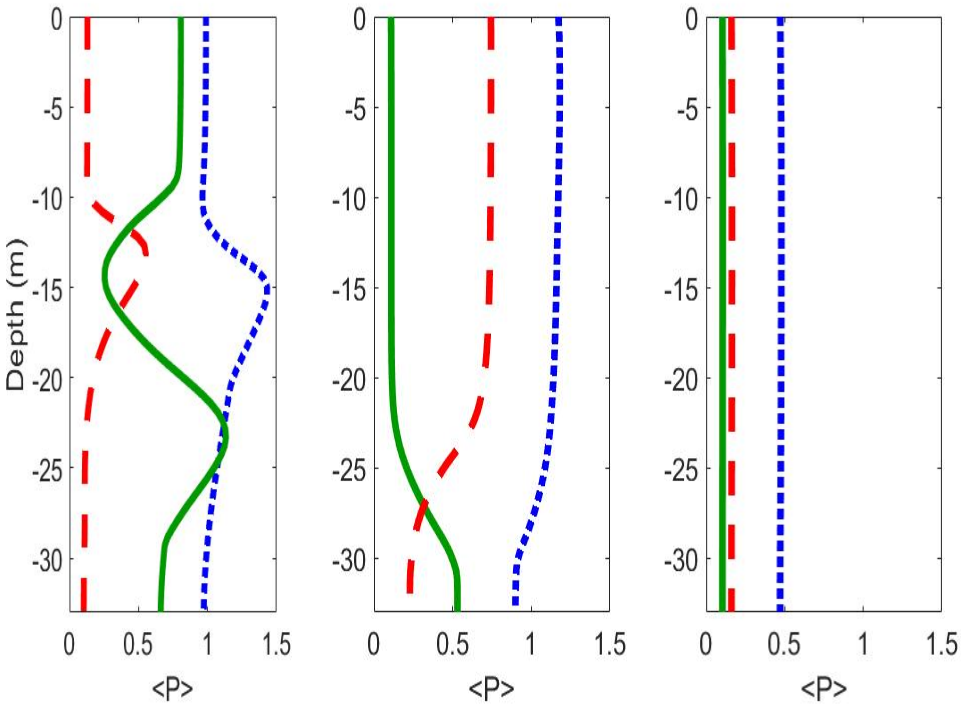

(a) Low wind (b) Intermediate wind (c) High wind

Figure 4: Depth profiles of $< P >$ at instantaneous points in time. The dotted (blue) line shows the profile after 3 days, the solid (green) line shows the profile at 10 days and the dashed (red) line shows the profile at 17 days. A comparison was made between a low wind stress ($U_* = 2 \times 10^{-3}\text{ms}^{-1}$), a moderate wind stress ($U_* = 3.5 \times 10^{-3}\text{ms}^{-1}$), and a high wind stress ($U_* = 5 \times 10^{-3}\text{ms}^{-1}$).

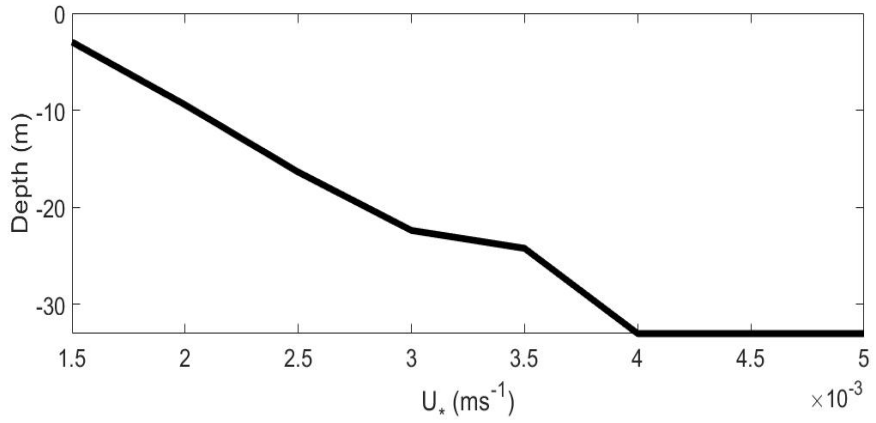

(a) Mixing depth z_{mix}

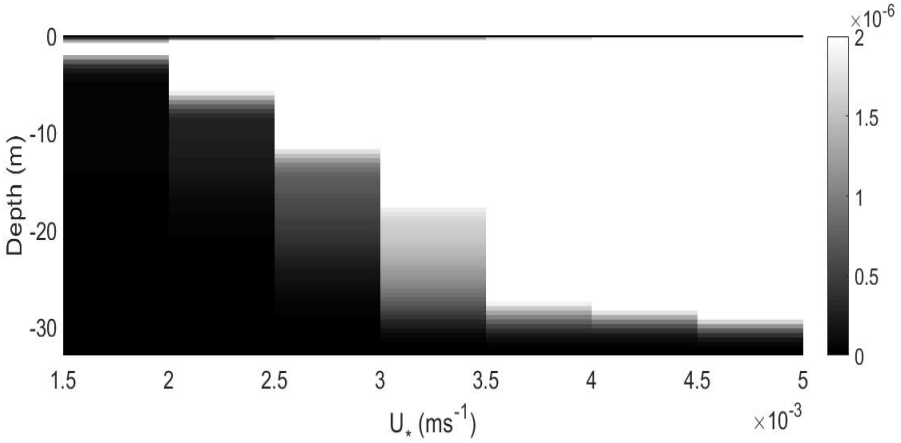

(b) $< w^2 >$

Figure 5: Mixing depth varying as a function of wind speed. Note here that for $U_* \geq U_{crit}$ and the vertical velocity variance $< w^2 >$ against depth, indicating vertical turbulent kinetic energy where lighter shades indicate higher energetics.

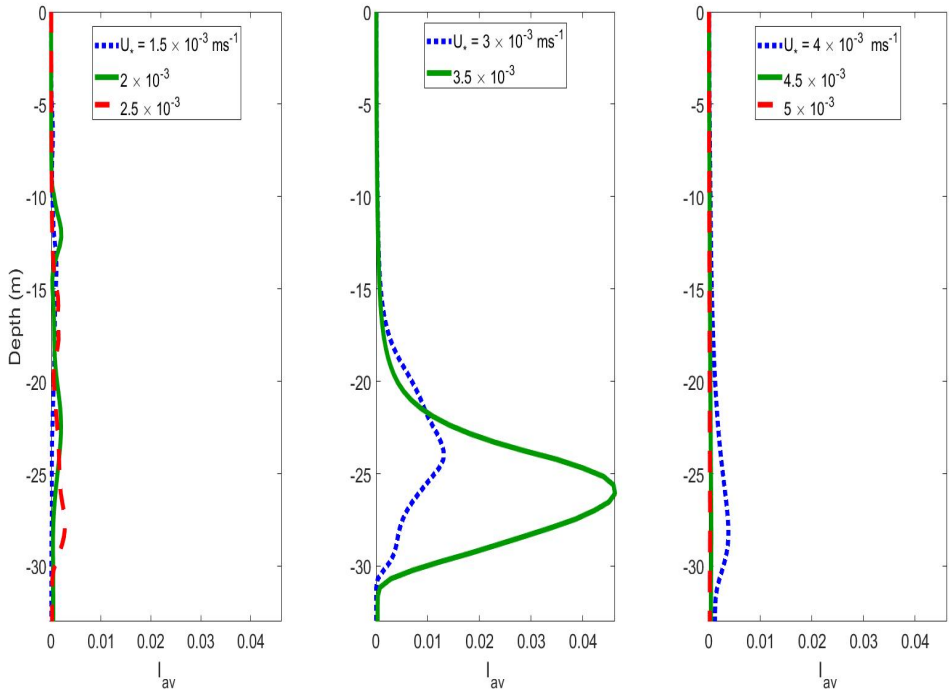

(a) Low wind (b) Intermediate wind (c) High wind

Figure 6: I_{av} (the quantification of lateral patchiness strength) ranging from low to high wind stress regimes. This illustrates the optimum condition for phytoplankton patchiness.

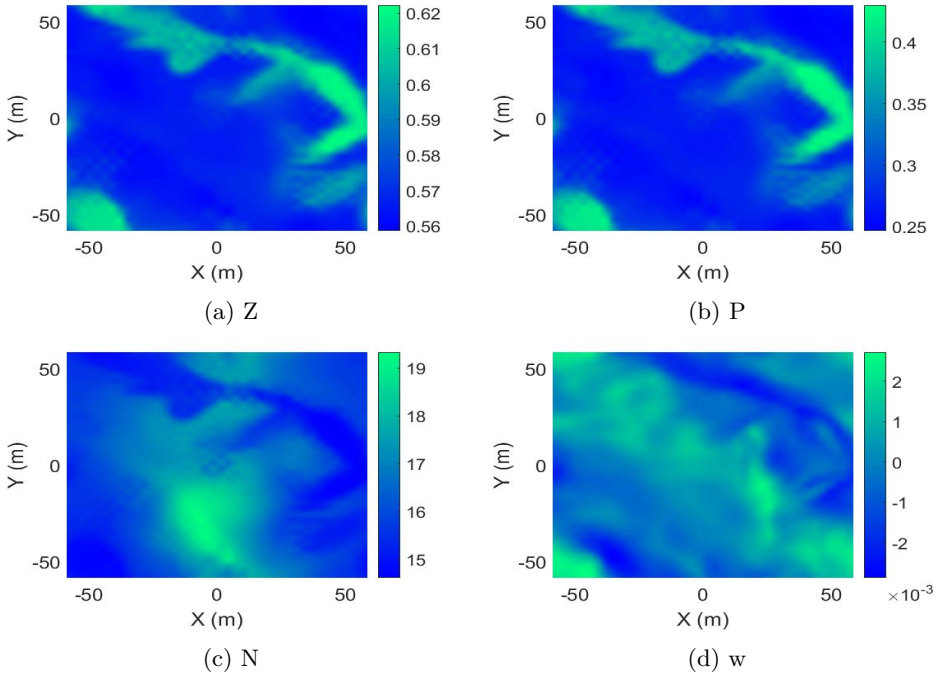

(a) Z (b) P

(c) N (d) w

Figure 7: Snapshot of Z, P, N and w at z_{opt} for an intermediate wind stress value of $U_* = 3.5 \times 10^{-3} \mathrm{ms}^{-1}$

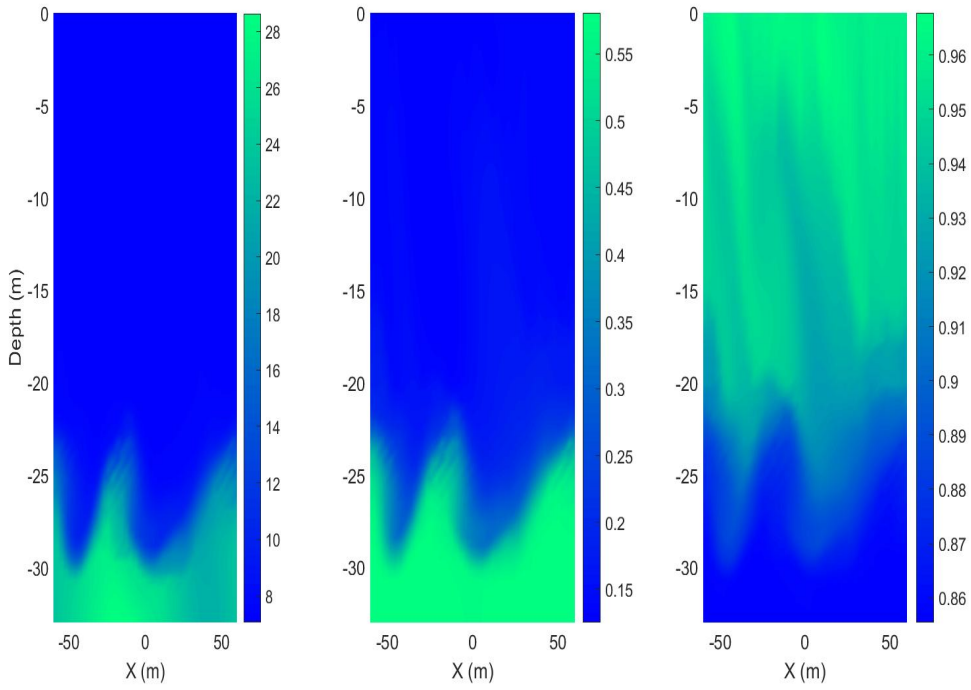

(a) N (b) P (c) Z

Figure 8: Nutrient, Phytoplankton and Zooplankton concentrations after 12 days of simulation time, when the Phytoplankton community are starting the bloom phase of the limit cycle. Here $U_* = 3.5 \times 10^{-3} ms^{-1}$

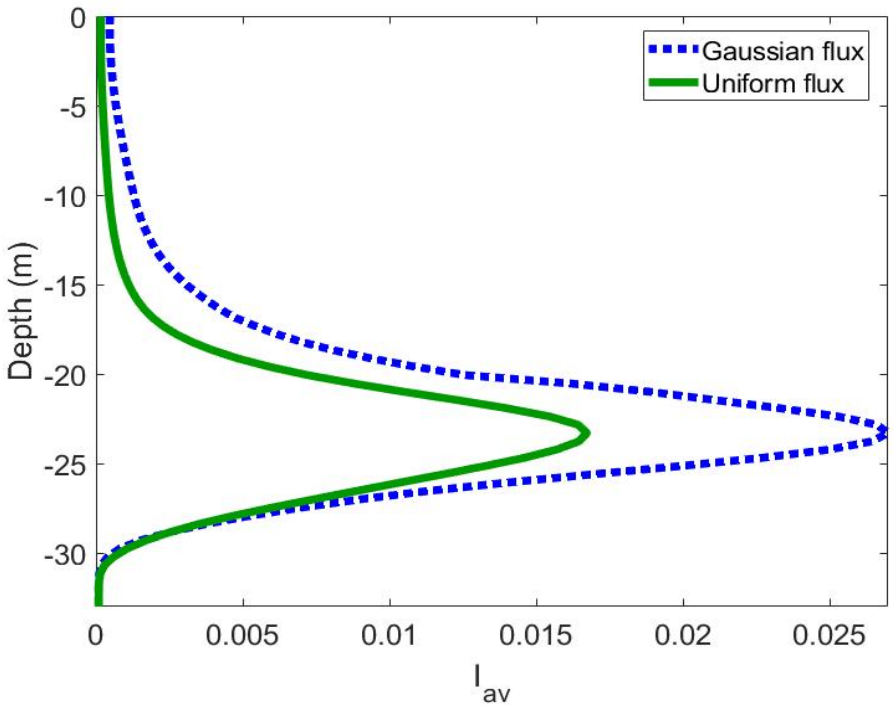

Figure 9: Graph of the time averaged patchiness intensity I_{av} against depth for $U_* = 3.5 \times 10^{-3} ms^{-1}$. The blue dotted line indicates a simulation prescribed by the Gaussian nutrient pump used in this work and the green solid line indicates a simulation prescribed by a uniform nutrient pump.

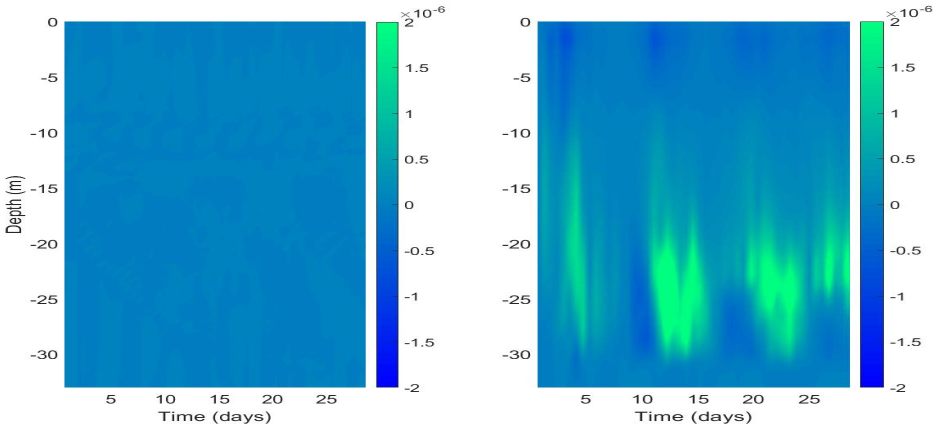

(a) Surface waves off

(b) Surface waves on

Figure 10: $< w'P' >$ for $U_* = 3.5 \times 10^{-3}\text{ms}^{-1}$. The left panel shows the correlation between vertical currents and Phytoplankton concentration with Langmuir circulations switched off and the right panel has Langmuir circulations switched on.